Navigation Functions Learning from Experiments: Application to Anthropomorphic Grasping

Ioannis F. Filippidis, Kostas J. Kyriakopoulos and Panagiotis K. Artemiadis

Abstract— **This paper proposes a method to construct Navigation Functions (NF) from experimental trajectories in an unknown environment. We want to approximate an unknown obstacle function and then use it within an NF. When navigating the same destinations with the experiments, this NF should produce the same trajectories as the experiments. This requirement is equivalent to a partial differential equation (PDE). Solving the PDE yields the unknown obstacle function, expressed with spline basis functions. We apply this new method to anthropomorphic grasping, producing automatic trajectories similar to the observed ones. The grasping experiments were performed for a set of different objects, Principal Component Analysis (PCA) allows reduction of the configuration space dimension, where the learning NF method is then applied.**

I. INTRODUCTION

There has been a sustained and increasing interest in creating autonomous robotic hands similar to the human hand, driven by manifold motivation. Contrary to industrial settings, in everyday human environments the majority of tasks involves objects adapted to human manipulation capabilities. Therefore an anthropomorphic robotic hand is uniquely suited to handling them. Applications include prosthetics [1], rehabilitation and teleoperation and dangerous tasks in hazardous or uninhabitable environments [2]. There are two main challenges in order to achieve this.

On the one hand, the required hardware needs to be developed. Several efforts witnessed in the past fifteen years started with four fingers, e.g. the Utah/MIT [3], DLR I [4] robotic hands and continued with five fingers, e.g. Anthrobot [5], Gifu II [6] and DLR/HIT II [7] hands. Some of the most difficult issues have been the reduction in size, increase of impact strength and of elasticity [8]. For a comparative overview see [9] and for a survey [10].

On the other hand, operation of these hands requires appropriate controllers. This is a motion planning problem in a configuration space (C-space) of high dimension. In addition, anthropomorphic movement may also be desirable in many cases. There have been several attempts to construct anthropomorphic controllers for robotic hands. The authors in [11], [12] treated a similar problem of anthropomorphic robot arm control by identifying joint dependencies using Dynamic Bayesian Networks (BN). In [13] BNs were applied to robot grasping learning. Identifying hand synergies through Principal Component Analysis (PCA) for grasping has been firstly proposed in [14] and *eigengrasps* are defined in [15].

Controlling a robotic hand in principal subspace has also been considered in [16], where eigengrasps are called Principal Motion Directions. The approach there is different from the one presented here, because free motion of the human hand instead of grasping is recorded, which does not provide information about everyday eigengrasps. Moreover, half of the measured configuration dimensions are not used, because PCA is performed after mapping human degrees of freedom (DOF) to robot hand DOF. Here PCA is applied to the full 22 DOF, independently of the robot hand.

Sampling-Based Roadmaps have been used in [16], which provide probabilistic completeness and are computationally intensive. The NF method is safe by construction, achieves provably correct convergence and offers a closed-loop continuous controller, integrating planning and trajectory tracking. Moreover, an NF captures anthropomorphism also within the principal subspace.

The contribution of the present work is in providing a new method for solving the inverse problem of motion planning, using Navigation Functions (NF). We assume that feasible trajectories are available after experimental measurements. We utilize these feasible trajectories to construct an obstacle function for the NF, through the solution of a PDE. This obstacle can then be used within the NF to navigate to destinations different than those of the experiments. The PDE requires that for the destinations of the experiments, the NF using this obstacle yields the same trajectories.

We then apply the new method to robot hand grasping, using 24 experiments of various grasping tasks for 13 different objects. PCA in the C-space enables considerable dimensionality reduction, by identifying a subspace spanned by the first principal components capturing most of the variability. Learning is performed in this principal subspace. This subspace also encodes anthropomorphism, as proved by the simulations.

The rest of this paper is organized as following: preliminaries about NFs are covered in § II, the problem is defined in § III and its inverse formulation using NFs developed in § IV, to be solved in § V. The method is applied to anthropomorphic grasping in § VI, where comparison with experiments supports its efficacy. Concluding remarks are summarized in § VII, where future research is considered.

Ioannis F. Filippidis and Kostas J. Kyriakopoulos are with the Control Systems Lab, Department of Mechanical Engineering, National Technical University of Athens, 9 Heroon Polytechniou Street, Zografou 15780, Greece. E-mail: jfilippidis@gmail.com, kkyria@mail.ntua.gr. Panagiotis K. Artemiadis is with the ASU Human-Oriented Robotics and Control Lab, School for Engineering of Matter, Transport and Energy, Ira A. Fulton Schools of Engineering, Arizona State University, USA. E-mail: panagiotis.artemiadis@asu.edu

This work has been supported by the European Commission with the Integrated Project no. 248587, THE Hand Embodied, within the FP7-ICT-2009-4-2-1 program Cognitive Systems and Robotics.

II. NAVIGATION FUNCTIONS

A. Background

Artificial Potential Fields were introduced by Khatib [17] and provide a closed-loop feedback controller for motion planning to avoid obstacles and safely reach the desired destination. This is achieved by following the negated gradient of an appropriately constructed scalar field. Obstacles are maxima and the destination the global minimum. Unfortunately, the appearance of local minima can trap the agent before reaching its destination.

Navigation Functions (NF) have been proposed by Rimon and Koditschek [18], [19] and overcome the local minima problem. Their initial formulation was for a priori known sphere worlds and application to geometrically more complicated worlds is achieved using diffeomorphisms [20]. These map the actual C-space obstacles to spheres. We have recently extended NFs to more general geometries in [21], without the need of diffeomorphisms. This enables the use of more complicated obstacles, like tori, ellipsoids and partially non-convex surfaces, as long as a curvature condition is satisfied. Utilizing this possibility, we explore the inverse problem of estimating unknown obstacles from knowledge of feasible trajectories.

B. Definition

Let $\beta \in C^2\left(E^n, \mathbb{R}\right)$ be a function over Euclidean space defining the union of obstacles $\mathscr{O} \triangleq \{q \in E^n | \beta(q) < 0\}$, such that the free space $\mathscr{F} \triangleq E^n \setminus \mathscr{O}$ be a compact connected analytic manifold with boundary.

An NF is defined on $\mathscr{F}$ as a map $\varphi : \mathscr{F} \to [0,1]$ which is at least C^2, admissible (uniformly maximal on the boundary), Morse (non-degenerate critical points) and Polar (unique global minimum at q_d). Such a function has been proved to exist for *every* $\mathscr{F}$ [18]. For a single integrator system, the control law

$$\frac{dx}{dt}(t) = -\nabla_q \varphi\left(x(t)\right) \tag{1}$$

solves the motion planning problem on $\mathscr{F}$ for almost all initial conditions on $\mathscr{F}$, apart from a Lebesgue measure zero set. But constructing one can prove to be demanding.

The following is one type of candidate NF proposed by Koditschek and Rimon [18], [19], hereafter called KRNF

$$\varphi(q, q_d) \triangleq \frac{\gamma_d(q, q_d)}{\left(\gamma_d(q, q_d)^k + \beta(q)\right)^{\frac{1}{k}}} \tag{2}$$

where $q \in \mathscr{F}$ the configuration, $\gamma_d(q, q_d) \triangleq \|q - q_d\|^2$ the paraboloid attractive effect and $k \in \mathbb{N} \setminus \{0, 1\}$ a tuning parameter. An example for φ is shown in Fig. 1a.

When $\mathscr{F}$ is an everywhere partially sufficiently curved world, as defined in [21], then there exists a $\hat{k}_{\min} > 0$, such that ϕ in Eq.(2) is a NF for all $k > \hat{k}_{\min}$ [21]. Sphere worlds are a special sub-category.

Here we construct an obstacle β which is *appropriate* to make the NF reproduce the experiments. Therefore, we formulate the inverse problem, whose solution is enforced to reproduce the measured speeds over the same paths. Hence, if the experimental speeds do not become zero, this is mathematically guaranteed to yield a NF for the configuration space subset that has been experimentally explored. The extension in [21] justifies the application of KRNFs to more complicated environments.

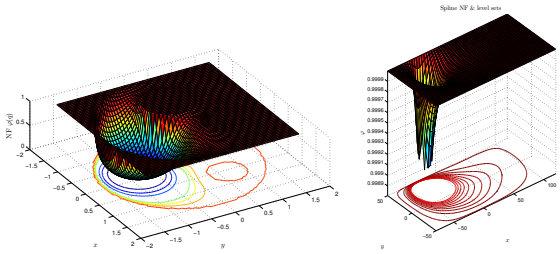

(a) Sample NF for $k = 2$. (b) Trained NF over 2D PCs.

Fig. 1: Navigation Function scalar fields.

III. PROBLEM DEFINITION

A. Definitions

Let $\mathbb{N}^* \triangleq \mathbb{N} \setminus \{0\}$, $I_e \triangleq \mathbb{N}^*_{\leq N_e}, I_i \triangleq \mathbb{N}^*_{\leq N_i}, N_e, N_i \in \mathbb{N}^*$. Assume that N_e trajectories are available, each with N_i configurations $x_i(t_j) \in \mathbb{R}^n$ and velocities $u_i(t_j) \triangleq \frac{dx_i}{dt}(t_j)$ measured in subsequent time instants t_j indexed in increasing order, where $i \in I_e, j \in I_i$. Also, assume that the desired destinations $q_{di} \in \mathbb{R}^n$ are provided. Note that if q_{di}, u_i are not provided, then we can always set $q_{di} = x_i(t_{N_i})$ and numerically differentiate $u_i(t_j) \triangleq \frac{x_i(t_{j+1}) - x_i(t_j)}{t_{j+1} - t_j}$, discarding the last configuration, because it lacks a corresponding u_i. Let $X_i \triangleq \{x_i(t_j)\}_{j \in I_i}, U_i \triangleq \{u_i(t_j)\}_{j \in I_i}$ denote the configuration and velocity functions of each sampled trajectory.

B. Problem Statement

The problem can then be stated as follows, Fig. 2. Using the above experimental data $E \triangleq \{X_i, U_i, q_{di}\}_{I_e}$ find a function $\beta \in C^2\left(E^n, \mathbb{R}\right)$ to satisfy equation

$$u_i(t_j) = -\nabla_q \varphi\left(x_i(t_j), q_{di}\right), \ \forall j \in I_i, \forall i \in I_e \tag{3}$$

subject to the positivity constraints on the sampled points

$$\beta\left(x_i(t_j)\right) > 0, \quad \forall j \in I_i, \quad \forall i \in I_e \tag{4}$$

and the workspace boundary $\partial\mathscr{W}$ closure requirement

$$\beta(q) \leq 0, \quad \forall q \in \partial\mathscr{W} \tag{5}$$

The positivity constraints in Eq.(4) follow from the obstacle definition $\beta(q) > 0, \forall q \in \mathring{\mathscr{F}}$ in the free space interior. The closure requirement of Eq.(5) ensures that the trajectories produced by the resulting controller will always remain within $\mathscr{W} \subset E^n$, the domain of our problem.

IV. INVERSE METHOD FORMULATION

In this section Eq.(3) is manipulated to derive an equivalent Partial Differential Equation (PDE) for the unknown obstacle function β, to be solved in § V.

In the problem formulation we have implicitly made the working hypothesis that a function of the form of Eq.(2) can

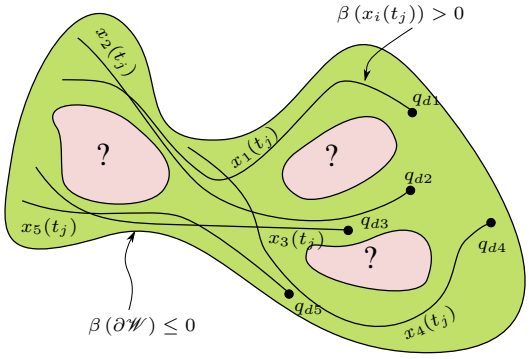

Fig. 2: Problem statement: obstacle approximation using experiments.

adequately represent a controller producing the experimental measurements recorded (or, equivalently, that a controller of this form exists, which can produce such trajectories). This is expressed by equating the measured velocity u to the gradient $-\nabla_q\varphi$ of the *candidate* Navigation Function φ at the corresponding measured configurations in Eq.(3), i.e.,

$$\begin{aligned}\nabla_q\varphi(q,q_d) &= \frac{\partial\varphi}{\partial\gamma_d}(\gamma_d,\beta)\nabla_q\gamma_d(q,q_d) + \frac{\partial\varphi}{\partial\beta}(\gamma_d,\beta)\nabla_q\beta(q)\\ \nabla_q\beta(q) &= \frac{\nabla_q\varphi(q,q_d) - \frac{\partial\varphi}{\partial\gamma_d}(\gamma_d,\beta)\nabla_q\gamma_d(q,q_d)}{\frac{\partial\varphi}{\partial\beta}(\gamma_d,\beta)}\end{aligned} \tag{6}$$

This is a PDE in the configuration q for the unknown obstacle function β. Substituting the experimental results of Eq.(3) in Eq.(6) leads to the equation

$$\begin{aligned}&\nabla_q\beta\left(x_i(t_j)\right) =\\ &-\frac{u_i(t_j) + \frac{\partial\varphi}{\partial\gamma_d}\left(\gamma_d\left(x_i(t_j),q_{di}\right),\beta\left(x_i(t_j)\right)\right)\nabla_q\gamma_d(x_i(t_j),q_{di})}{\frac{\partial\varphi}{\partial\beta}\left(\gamma_d\left(x_i(t_j),q_{di}\right),\beta\left(x_i(t_j)\right)\right)}\end{aligned} \tag{7}$$

for all $j \in I_i$, for all $i \in I_e$. In this equation $u_i(t_j)$ is known from experimental measurements, $\frac{\partial\varphi}{\partial\gamma_d}, \frac{\partial\varphi}{\partial\beta}$ are also known functions of $\gamma_d(q,q_d)$ and $\beta(q)$ (for a specific $\varphi(\gamma_d,\beta)$) and $\gamma_d, \nabla_q\gamma_d$ are also known functions of the experimental $x_i(t_j), q_{di}$. As a result, we can substitute $x_i(t_j), u_i(t_j), q_{di}$ to obtain a PDE which contains as unknowns only function β and its derivative $\nabla\beta$. This then constitutes a PDE to solve in the unknown obstacle function $\beta : \mathbb{R}^n \to \mathbb{R}$ under the constraints imposed by Eq.(4) and Eq.(5). When a paraboloid attractive function γ_d is used, then $\nabla\gamma_d(q) = 2(q - q_d)$. To proceed further, we first need to select a specific form for NF φ.

By selecting a NF formula φ we can substitute the partial derivatives $\frac{\partial\varphi}{\partial\gamma_d}, \frac{\partial\varphi}{\partial\beta}$ in Eq.(7). For the φ of Eq.(2) we obtain

$$\frac{\partial\varphi}{\partial\gamma_d} = \beta\left(\gamma_d^k + \beta\right)^{-\frac{1}{k}-1}, \quad \frac{\partial\varphi}{\partial\beta} = -\frac{1}{k}\gamma_d\left(\gamma_d^k + \beta\right)^{-\frac{1}{k}-1}$$

so substitution in Eq.(7) yields

$$\nabla\beta = \left(k\frac{u_i}{\gamma_d}\right)\left(\gamma_d^k + \beta\right)^{\frac{1}{k}+1} + \left(k\frac{\nabla\gamma_d}{\gamma_d}\right)\beta \tag{8}$$

which holds on the trajectory points $x_i(t_j)$. This is a system of first order semi-linear variable-coefficient partial differential equations. Its solution is described in § V.

V. SOLUTION

A. Setup

1) Splines: Basis splines (B-Splines) [22] were selected as the solution basis, because they can be as smooth as needed and form a polynomial approximation. Appropriate knot density can ensure that the solution is sufficiently approximated and the B-form implicitly incorporates smoothness constraints, remaining differentiable for varying coefficients, contrary to the Piecewise polynomial form. Therefore, the solution is searched in the finite-dimensional space of B-spline coefficients, where

$$\beta(q) = \sum_{i_1=1}^{m_1}\sum_{i_2=1}^{m_2}\cdots\sum_{i_n=1}^{m_n}\left(c_{i_1 i_2\ldots i_n}\prod_{r=1}^{n}B\left(q_r|t_r\right)\right) \tag{9}$$

with $\beta \in C^2(D,\mathbb{R})$ is the interpolated obstacle function over the domain $D \subset \mathbb{R}^n$, $q \in \mathbb{R}^n$ is the system's configuration, $q_r \in \mathbb{R}$ denotes the r^{th} component of q,

$$C \triangleq \{c_{i_1 i_2\ldots i_n}\}_{i_j \in \mathbb{N}^*_{\leq m_j}, j\in\mathbb{N}^*_{\leq n}} \in \times_{j\in\mathbb{N}^*_{\leq n}}\mathbb{R}^{m_j}$$

is the coefficient tensor,

$$\begin{aligned}t &= [t_{ri_r},\, t_{r(i_r+1)},\,\ldots,\,t_{r(i_r+h_r)}]\\ t_{ij} &\in \mathbb{R}, i \in \{1,2,\ldots,n\}, j \in \{1,2,\ldots,m_i+h_i\}\end{aligned}$$

are the knot sequences of each dimension and $h_i \in \mathbb{R}, i \in \mathbb{N}^*_{\leq n}$ are the orders of the splines of each dimension and $B(q_r|t_r)$ are the basis functions. Let us also stack the coefficient tensor in a vector of *design variables* for the minimization problem

$$\begin{aligned}c \triangleq\ &[c_{11\cdots1}, c_{21\cdots1}, \ldots, c_{m_1 1\ldots1},\\ &c_{12\ldots1}, c_{22\ldots1}, \ldots, c_{m_1 2\ldots1}, \ldots, c_{m_1\ldots m_n}]^{\mathrm{T}}\end{aligned} \in \mathbb{R}^{\sum_{i=1}^{n} m_i}$$

2) Domain of definition: The domain of definition $\mathscr{W}$ is selected based on the variable limits of the problem under consideration. Selection of an appropriate domain is important because if its boundary $\partial\mathscr{W}$ is more than a knot away from the closest trajectory point, then the boundary closure Eq.(5) is implicitly satisfied during solution, provided the initial iteration has $\beta(\partial\mathscr{W}) = 0$. This follows because perturbations of B-spline coefficients corresponding to boundary knots do not affect the collocation error on the experimental trajectories.

3) Knot allocation over dimensions: For each dimension the recorded trajectories exhibit different variance. The number of B-spline knots allocated to each dimension is chosen proportionally to the associated experimental variance. This efficiently allocates more knots to dimensions where more variability needs to be represented.

B. Iterative semi-linear PDE system solution

To solve the semi-linear PDE of Eq.(8) under the positivity constraints of Eq.(4) an iterative gradient descent algorithm [23] $c^{N+1} = c^N - \lambda_J\nabla_c J$ has been used, minimizing the error functional J described in § V-B.2. The positivity constraints are also incorporated in this functional, while the boundary closure constraints Eq.(5) are implicitly satisfied, as already described.

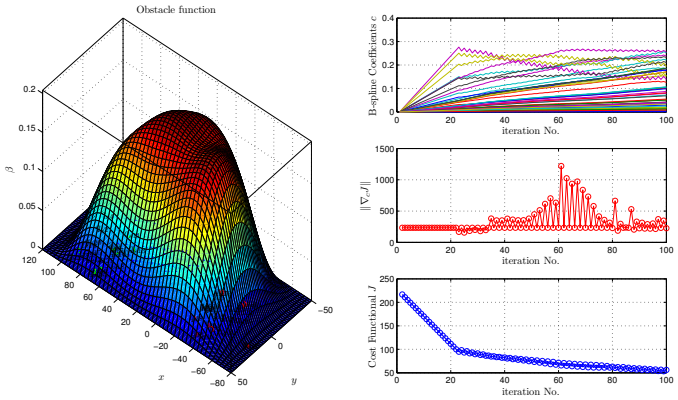

Fig. 3: Obstacle function β from PDE solution using $N_e = 24$ experiments.

1) Initial point: A flat obstacle $\beta \equiv 0$ is used as the initial solution. Therefore, during the initial iteration, the main effect originates in the terms J_{sp}, J_{dp} of the cost functional, which are defined in the next subsection.

2) Optimization Cost Functional: The appropriate choice of functional $J : C^2(D, \mathbb{R}) \times D_e \to [0, +\infty)$ is crucial for the successful solution for β. The cost functional used is

$$J \triangleq \frac{1}{\sum_{i \in I_e} N_i} \left(w_1 J_{PDE} + w_2 J_{sp} + w_3 J_{dp} + w_4 J_{bn} \right)$$

$$J_{PDE} \triangleq \sum_{i \in I_e, j \in I_i} \Delta E_{ij}, J_{sp} \triangleq \sum_{i \in I_e, j \in I_i} s\left(\beta\left(x_i(t_j)\right) - \beta_0\right)$$

$$J_{dp} \triangleq \sum_{q_{di}, i \in I_e} s\left(\beta(q_{di}) - \beta_0\right), J_{bn} \triangleq \sum_{q_n \in \partial \mathcal{W}} s\left(\beta(q_n)\right)$$

where $w_i \in (0, +\infty), i \in \{1, 2, 3, 4\}$ are weighting factors, offsets β_0 is a numerical threshold above which β is considered positive, function $s : \mathbb{R} \to \mathbb{R}$ is a C^2-smooth switch $s(x) \triangleq \begin{cases} x^3, x \leq 0 \\ 0, 0 < x \end{cases}$ and the component functionals are described hereafter. The satisfaction error of the PDE system of Eq.(8) is accounted for in J_{PDE} as

$$\Delta E_{ij} \triangleq \frac{1}{\gamma_d^k} \left\| \nabla\beta - \left(k \frac{u_i}{\gamma_d}\right) \left(\gamma_d^k + \beta\right)^{\frac{1}{k}+1} - \left(k \frac{\nabla\gamma_d}{\gamma_d}\right) \beta \right\|_2^2$$

where term γ_d^k ensures a fair weighting along the trajectory.

Functional J_{sp} enforces positivity at the sampled points, i.e., the condition of Eq.(4). Positivity at the destinations is ensured by J_{dp}. Domain closure of Eq.(5) is imposed by the boundary non-positivity functional J_{bn}. Here $w_4 = 0$ for reasons explained in § V-A.2. The optimization for the case study in § VI is shown in Fig. 3.

C. Constructed controller

For a selected destination $q_d \in \beta^{-1}((0, +\infty))$ the control law is $u_c(t) = -\nabla_q \varphi\left(x(t)\right)$ which yields

$$u_c(t) = -\frac{\beta(x) \nabla_q \gamma_d(x, q_d) - \frac{\gamma_d(x, q_d)}{k} \nabla_q \beta(x)}{\left(\gamma_d(x, q_d)^k + \beta(x)\right)^{\frac{1}{k}+1}}$$

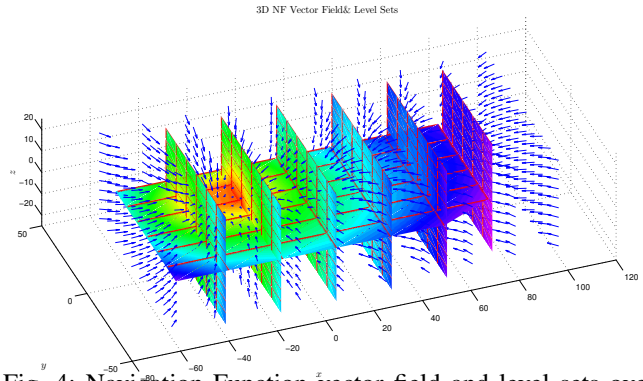

Fig. 4: Navigation Function vector field and level sets over 3D PC space.

TABLE I: Grasping Experiments

No.	Object	Task
1,2,3,4	Tall glass	Grasp: to drink, from side & move from top & move, from side & rotate
5, 6, 7	Mouse	Grasp to: slide, left click, right click
8,9,10,11	Cup	same as tasks as 1,2,3,4
12	Hammer	Grasp to use
13	Ashtray	Grasp from above to move
14	Cube	Grasp from above to raise
15, 16	Pen	Write, Move
17, 18	Jar	Move, Lid unscrewing
19	Screwdriver	Grasp to operate
20	Book	Grasp from right side to read
21	Mobile phone	Pick up to view
22, 23	Scissor	Grasp to: Move, Use
24	Stapler	Grasp and use

where x is the system's state. The potential field and level sets of a 2-dimensional controller for a selected q_d are shown in Fig. 1b and of a 3-dimensional controller in Fig. 4.

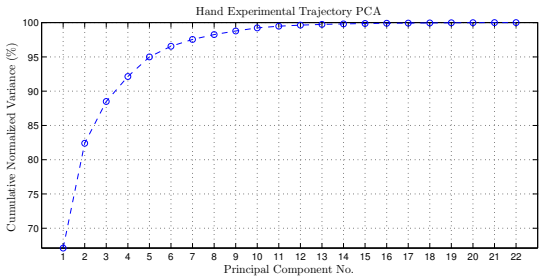

Fig. 5: PCA cumulative normalized variances.

VI. APPLICATION TO ANTHROPOMORPHIC ROBOTIC HAND CONTROL

A. Experimental procedure

The $N_e = 24$ grasping experiments of Table I have been conducted with one subject grasping 13 different objects using its right hand. Multiple tasks have been performed for 6 of the objects. Snapshots of the experimental setup are shown in Fig. 8 and a video accompanies this work. The hand angles have been measured using a CyberGlove data glove [24], which features electric angle sensors with 1° resolution and records 22 degrees of freedom at a 100 Hz sampling rate, 3 flexions/extensions for each finger apart from the thumb,

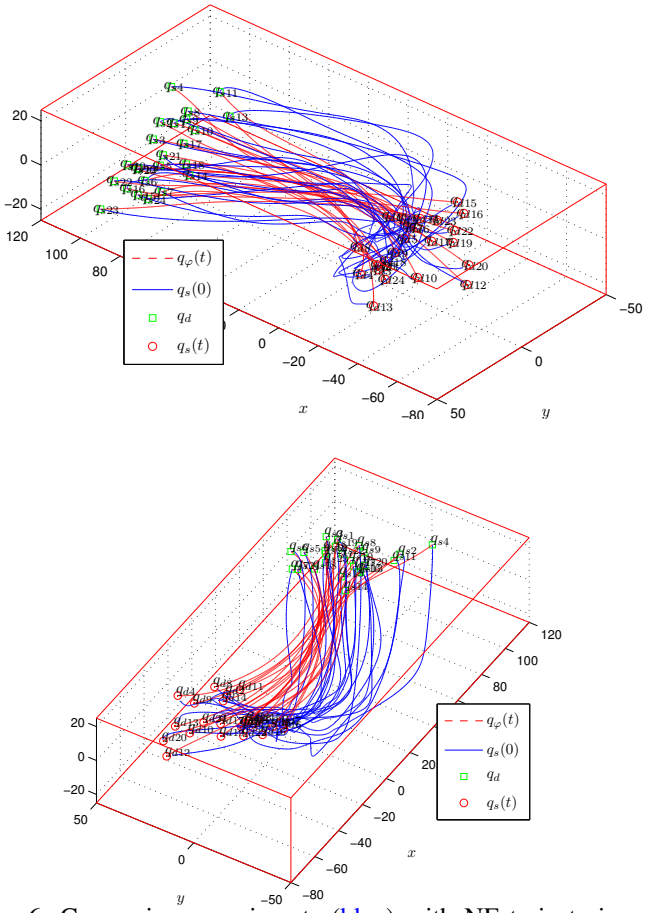

Fig. 6: Comparing experiments (blue) with NF trajectories (red), using the *same* obstacle β for all of them, over the first 3 Principal Components. Initial conditions are q_{si} (green squares) and destinations are q_{di} (red circles).

for which they are 2, 1 ab/adduction, palm arch and 2 wrist degrees of freedom.

B. Principal Component Analysis

As is customary in the analysis of hand arm systems [14], [15], [11], Principal Component Analysis [25] is applied. Projecting the experimental data on the subspace spanned by the 3 principal components with the greatest variance reduces the high C-space dimension (22 measured angles) and captures 88.5% of the original variability, Fig. 5. The eigengrasps are shown in Fig. 7.

C. PDE Solution

A $2D$ B-spline obstacle function obtained by solving the PDE is shown in Fig. 3, together with the cost functional J, the design variable gradient norm $\|\nabla_c J\|$, where c are the B-spline coefficients in which the minimization takes place, and the B-spline coefficient variations throughout the optimization procedure. The cost functional J exhibits a smooth convergence to its minimum, which indicates robustness of the numerical problem. We provide more examples in [28]. Note that in Fig. 6 the trained obstacle is 3-dimensional.

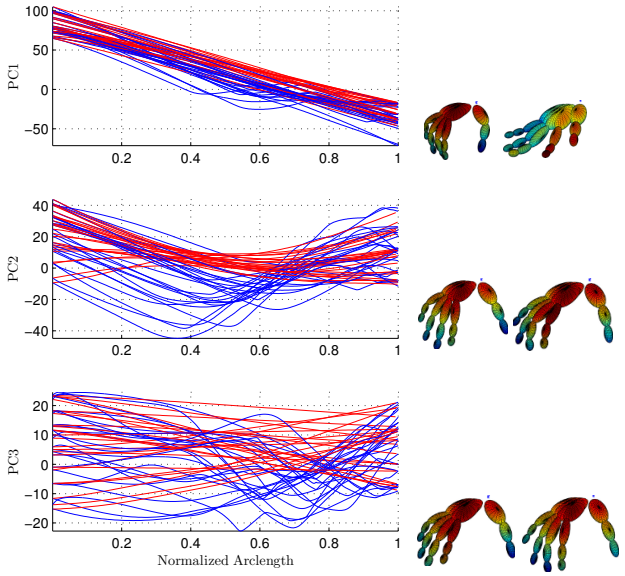

Fig. 7: Normalized arclength parameterization of PCs for experimental and NF generated trajectories, together with eigengrasps.

Fig. 8: Experimental setup during reach to grasp.

D. Comparison to experimental trajectories

A sequence of hand postures automatically generated using the NF on the 3-dimensional Principal Subspace of Fig. 6 is illustrated in Fig. 9. The hand destination configuration has been selected to grasp a tall glass, similarly to the first three experiments. The resultant reach-to-grasp trajectory of the system is smooth and reproduces anthropomorphism in a natural way. The first 3 principal components of experimental trajectories are compared with those generated by the NF in Fig. 7. Each trajectory is parameterized by its normalized arclength in the interval $[0, 1]$, for geometric comparison.

The human hand kinematic model described in [26] has been used, with parametrically defined lengths, as functions of the human hand length H_L and hand breadth H_B and phalanges modeled as ellipsoids [27]. More details concerning the kinematic model used can be found in [28].

Since only the hand is controlled in reach to grasp movements, it is not unexpected that a relatively low dimensional subspace suffices to produce such motion [14]. Moreover, note that the approximated obstacle in this case does *not* correspond to the C-obstacle arising due to the grasped objects during the experiments. The aim here is to capture the way a human moves, by means of a "virtual obstacle".

As far as arm movement is concerned, it correlates with hand movement [29] and this allows us to combine the methodology proposed here with previous work on anthropomorphic arm control [11], for fully automatic control

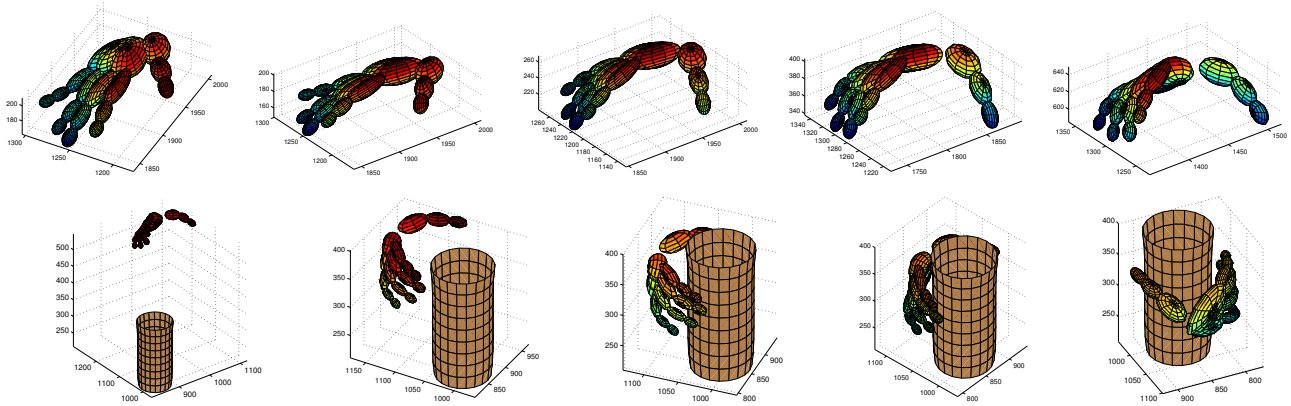

Fig. 9: Automatically generated grasping movement using Navigation Function in 3-dimensional principal subspace of Fig. 6, compare to Fig. 8.

of the complete hand-arm system. Alternative applications include hand prosthesis [15], where the subject provides wrist movement and the controller can select the appropriate configuration on the generated NF trajectory, based on correlations with EMG signals and wrist proximity to object.

VII. CONCLUSIONS AND FUTURE WORK

A method has been presented to construct Navigation Functions from experimental measurements. This is achieved by approximating an implicit obstacle function. This solution is obtained in terms of splines after the iterative solution of a nonlinear system of PDEs. Future work involves optimally mapping generated movements to robotic hands different than the human one and extension of the new method to arm-hand system control.

REFERENCES

[1] H. Huang, L. Jiang, Y. Liu, L. Hou, H. Cai, and H. Liu, "The mechanical design and experiments of hit/dlr prosthetic hand," in *IEEE Int. Conf. on Robotics and Biomimetics*, 2006, pp. 896–901.

[2] M. Diftler, J. Mehling, M. Abdallah, N. Radford, L. Bridgwater, A. Sanders, R. Askew, D. Linn, J. Yamokoski, F. Permenter, B. Hargrave, R. Platt, R. Savely, and R. Ambrose, "Robonaut 2 - the first humanoid robot in space," in *Proc. IEEE Int. Conf. on Rob. and Aut.*, 2011, pp. 2178–2183.

[3] S. Jacobsen, J. Wood, D. Knutti, and K. Biggers, "The utah/m.i.t. dextrous hand: Work in progress," *Int. J. of Rob. Reasearch*, vol. 3, no. 4, pp. 21–50, 1984.

[4] J. Butterfass, G. Hirzinger, S. Knoch, and H. Liu, "Dlr's multisensory articulated hand. i. hard- and software architecture," in *Proc. IEEE Int. Conf. on Rob. and Aut.*, vol. 3, 1998, pp. 2081–2086.

[5] K. Kyriakopoulos, J. Van Riper, A. Zink, and H. Stephanou, "Kinematic analysis and position/force control of the anthrobot dextrous hand," *IEEE Trans. on Systems, Man, and Cybernetics, Part B: Cybernetics*, vol. 27, no. 1, pp. 95 –104, 1997.

[6] T. Mouri, T. Endo, and H. Kawasaki, "Review of gifu hand and its application," *Mechanics Based Design of Structures and Machines*, vol. 39, no. 2, pp. 210–228, 2011.

[7] H. Liu, K. Wu, P. Meusel, N. Seitz, G. Hirzinger, M. Jin, Y. Liu, S. Fan, T. Lan, and Z. Chen, "Multisensory five-finger dexterous hand: The dlr/hit hand ii," in *IEEE/RSJ Int. Conf. on Intell. Rob. and Sys.*, 2008, pp. 3692–3697.

[8] S. Wolf, O. Eiberger, and G. Hirzinger, "The dlr fsj: Energy based design of a variable stiffness joint," in *Proc. IEEE Int. Conf. on Rob. and Aut.*, 2011, pp. 5082–5089.

[9] C. Rosales, L. Ros, J. Porta, and R. Surez, "Synthesizing grasp configurations with specified contact regions," *The Int. J. of Rob. Research*, vol. 30, no. 4, pp. 431–443, 2011.

[10] A. Bicchi, "Hands for dexterous manipulation and robust grasping: a difficult road toward simplicity," *IEEE Trans. on Rob. and Aut.*, vol. 16, no. 6, pp. 652 –662, 2000.

[11] P. Artemiadis, P. Katsiaris, and K. Kyriakopoulos, "A biomimetic approach to inverse kinematics for a redundant robot arm," *Auton. Rob.*, vol. 29, pp. 293–308, 2010.

[12] P. Katsiaris, P. Artemiadis, and K. Kyriakopoulos, "Modeling anthropomorphism in dynamic human arm movements," in *IEEE/RSJ Int. Conf. on Intell. Rob. and Sys.*, 2010, pp. 3507–3512.

[13] D. Song, C. Ek, K. Huebner, and D. Kragic, "Multivariate discretization for bayesian network structure learning in robot grasping," in *Proc. IEEE Int. Conf. on Rob. and Aut.*, 2011, pp. 1944–1950.

[14] M. Santello, M. Flanders, and J. Soechting, "Postural hand synergies for tool use," *The J. of Neuroscience*, vol. 18, no. 23, pp. 10 105–10 115, 1998.

[15] M. Ciocarlie and P. Allen, "Hand posture subspaces for dexterous robotic grasping," *The Int. J. of Rob. Research*, vol. 28, no. 7, pp. 851–867, 2009.

[16] J. Rosell, R. Surez, C. Rosales, and A. Prez, "Autonomous motion planning of a hand-arm robotic system based on captured human-like hand postures," *Auton. Rob.*, vol. 31, pp. 87–102, 2011.

[17] O. Khatib, "Real-time obstacle avoidance for manipulators and mobile robots," *Int. J. of Rob. Research*, vol. 5, no. 1, pp. 90–98, 1986.

[18] D. E. Koditschek and E. Rimon, "Robot navigation functions on manifolds with boundary," *Adv. in Applied Math.*, vol. 11, pp. 412–442, 1990.

[19] E. Rimon and D. E. Koditschek, "Exact robot navigation using artificial potential functions," *IEEE Trans. on Rob. and Aut.*, vol. 8, no. 5, pp. 501–518, 1992.

[20] ——, "The construction of analytic diffeomorphisms for exact robot navigation on star worlds," *Trans. of the Am. Math. Soc.*, vol. 327, no. 1, pp. 71–116, 1991.

[21] I. F. Filippidis and K. J. Kyriakopoulos, "Navigation functions for everywhere partially sufficiently curved worlds," in *IEEE Int. Conf. on Rob. and Aut.*, St. Paul, MN, USA, 2012.

[22] C. de Boor, *A Practical Guide to Splines*. Springer, 2001.

[23] R. Fletcher, *Practical Methods of Optimization*. Wiley, 2000.

[24] CyberGlove Systems LLC, *CyberGlove® Data Glove: User Guide*, 1st ed., Dec. 2007.

[25] I. Jolliffe, *Principal Component Analysis*, 2nd ed. Springer, 2002.

[26] E. Pitarch, "Virtual human hand: Grasping strategy and simulation," Ph.D. dissertation, Univ. Politecnica de Catalunya, 2007.

[27] B. Buchholz and T. Armstrong, "A kinematic model of the human hand to evaluate its prehensile capabilities," *J. of Biomechanics*, vol. 25, no. 2, pp. 149 – 162, 1992.

[28] I. Filippidis, "Navigation functions for unknown sphere worlds, general geometries, their inverse problem and combination with formal methods," Diploma Thesis, Dept. of Mech. Eng., National Tech. Uni. of Athens, 2011.

[29] C. E. Vargas-Irwin, G. Shakhnarovich, P. Yadollahpour, J. Mislow, M. Black, and J. Donoghue, "Decoding complete reach and grasp actions from local primary motor cortex populations," *The J. of Neuroscience*, vol. 30, no. 29, pp. 9659–9669, 2010.